Influence of nanoparticle doping on electronic properties of MgB2 bulk samples

Influence of nanoparticle doping on electronic properties of MgB_2 bulk samples

Journal of Physics: Conference Series **234** (2010) 012014 doi:10.1088/1742-6596/234/1/012014

Influence of nanoparticle doping on electronic properties of MgB_2 bulk samples

L Gozzelino[1], R Gerbaldo[1], G Ghigo[1], F Laviano[1], G Lopardo[1], E Mezzetti[1], G A Ummarino[1], G Giunchi[2], E Perini[2], L Saglietti[2], E Bassani[3] and B Minetti[1]

[1] Dept. of Physics, Politecnico Torino, C.so Duca degli Abruzzi 24, 10129 Torino, Italy

[2] EDISON SpA, R&D Dept., Foro Buonaparte 31, 20121 Milano, Italy

[3] CNR-IENI, Lecco Labs., Corso Promessi Sposi 29, 23900 Lecco – Italy

E-mail: laura.gozzelino@polito.it

Abstract. Superconducting and normal-state properties of MgB_2 polycrystalline samples with non magnetic (SiC) and magnetic (Co) dopant addition were analysed in order to study the doping influence on the magnetic anisotropy of MgB_2 polycrystalline samples and to correlate this influence with the doping-induced changes in band scattering processes. Both doping typologies result in a decrease of the MgB_2 upper critical field anisotropy factor. For SiC-doped samples this result is joined to an upper critical field (B_{c2}) shift toward higher temperatures whereas Co doped samples exhibit a B_{c2} decrease. To guide the application road map a theoretical approach to the analysis of the normal state resistivities (SiC doping) and of the upper critical field dependence on temperature (SiC and Co dopings) was performed. According to this scenario, band scattering rate as well as electron diffusivity values obtained by these analyses showed for both the investigated doping typologies an increase of intraband scattering processes in the more anisotropic σ band whereas the conductivity of π band remains almost unaffected.

1. Introduction

Superconducting- and normal-state properties of MgB_2 were found to be strongly influenced by its multiband-band electronic structure - that can be approximated by one quasi-2D σ band and one 3D π band with different energy gaps - and the consequent intraband and interband scattering mechanisms [1-4]. Doping with different elements or compounds [2, 3, 5] is the most promising solution for a controlled disorder introduction inside MgB_2 that, affecting both intraband and interband scattering processes, changes its superconducting and normal-state properties and allows the production of more and more competitive material. The best results in the enhancement of critical parameters such as the upper critical field (B_{c2}) and the critical current density (J_c) as well as in the reduction of the material intrinsic anisotropy were obtained with pure carbon [6-11] as well as with organic (carbohydrates [12-14]) and carbonaceous inorganic compound (SiC, B_4C [15, 9, 16-18]) doping but also additions of different metallic elements were successfully attempted [19-24].

However the development of more and more efficient doping procedures cannot leave the knowledge of the doping effect on the band conduction regime out of consideration. The analysis of

the dependence on temperature of the normal state resistivity as well as of the upper critical field are among the best techniques to get information on the MgB_2 electron transport properties. The fit with the $\rho = \rho_0 + aT^m$ law allows one to probe the influence of electron-phonon and inter-electron scattering processes [5, 25, 26] whereas the fit with the classical Block-Grüneisen expression allows obtaining the Debye temperature of the compound as well as the strength of the electron-phonon coupling [26, 27] and the band contribution to the current transport [28]. Moreover, assuming a negligible interband scattering, the multiband model proposed by Mazin *et al.* [29] allows evaluating the σ and π intraband scattering rates from the analysis of the resistivity behaviour [30]. On the other hand average Fermi velocities can be obtained by the analysis of the temperature dependence of the upper critical field in the framework of the Eliashberg model [31-33] whereas band electronic diffusivities can be directly calculated by applying the models formulated by Gurevich [34] and Golubov and Koshelev [35].

In this paper we focus on the role of low-level C doping by SiC nanoparticles and Co doping in affecting the anisotropy of magnetic properties of MgB_2 polycrystalline samples and on how this anisotropy variation finds its counterparts in the change of band scattering processes. The samples were grown by the Reactive Mg Liquid Infiltration (Mg-RLI) technique [36] that allows producing MgB_2 manufacts of suitable sizes and shapes to take into account applicative tools such as magnetic bearings, flywheels, magnetic shields [37].

Firstly the non-magnetic and magnetic doping influence on B_{c2} anisotropy factor, calculated by the irreversibility (B_{irr}) and upper critical field analysis within the percolation model proposed by Eisterer *et al.* [5, 38], is described. The influence on B_{c2} dependence on temperature is discussed, too. These doping effects on macroscopic electrical transport properties are then correlated with the doping-induced changes in band conduction parameters. Aiming at this the SiC-induced non-magnetic impurity influence on band scattering rates, obtained by applying the model formulated by Mazin *et al*. [29] to the analysis of the normal state resistivities, is presented and compared with the effects on electronic diffusivities determined from the study of the B_{c2} vs. T behaviour within the model suggested by Gurevich [34]. Then Co-magnetic doping influence on band scattering rates, evaluated by the analysis of the B_{c2} vs. T curves in the framework of the Eliashberg theory [55], is outlined and discussed.

2. Experimental details

2.1. Growth details

MgB_2 bulk samples were cut in parallelepiped bars (0.5-1 x 1-2 x 12 mm^3) from large pellets obtained by the Mg-RLI technique. This growth process offers several technological advantages: a) it does not require hot high pressure machine but a conventional oven, b) it can be performed with a common metallic containers and c) it allows producing manufactures with size larger than ten centimetres suitably shaped to take into account different applicative tools [37].

Undoped samples were prepared starting from the elemental compound B (99.5% of purity) and Mg (99.9 % of purity) by means of a thermal treatment at T = 900°C. After cooling the resulting MgB_2 manufact occupies almost all the space initially filled by the B powder. More details on the growth procedure are reported elsewhere [36, 39].

SiC-doped samples were obtained mixing a stoichiometric amount of Mg with a mixture of B powders added with 10%wt of nanosized SiC powders with size of about 20-30 nm. X-ray diffraction pattern reveals a small shift of the (hk0)-type MgB_2 peaks indicating a contraction of the *a* axis of the crystal lattice of about 0.10 %, as expected in presence of small C substitution on boron site [40]. No new phases, such as Mg_2Si, BC or MgB_2C_2 were detected [41]. This means that only a small fraction of carbon entered the MgB_2 cell whereas the remnant part of the dopant stayed located at the grain boundaries.

TABLE I. Critical temperatures, residual resistivity ratios and lattice parameters of the three investigated sample typologies

	undoped	SiC-doped	Co-doped
T_c (K)	38.80 ± 0.05	38.50 ± 0.05	36.45 ± 0.05
RRR	5.0	5.4	4.2
a axis (Å)	3.085 ± 0.001	3.081 ± 0.001	3.083 ± 0.001
c axis (Å)	3.523 ± 0.002	3.519 ± 0.003	3.521 ± 0.002

Co-doped samples were prepared by mixing microcrystalline B with an over-stoichiometric amount of Mg-Co alloy (nominal 5wt% of Co). In agreement with [42] *a* and *c* axis of the crystal lattice keeps substantially the same values of the undoped MgB_2. This does not rule out that a small percentage of Co enters the MgB_2 cell on Mg sites since the Co atomic radius is similar to the Mg one.

In both cases growth procedure of doped samples was similar to that of the undoped ones.

In this paper we present the characterization of three samples representative of the three sample typologies: undoped, SiC-doped and Co-doped.

2.2. Electric transport measurement details

Sample resistivities, ρ, were measured using a standard four-probe technique. Magnetic field was applied perpendicularly to the current direction. The critical temperatures, T_c, evaluated from the resistive-transition inflection-point and the residual resistivity ratios, RRR, calculated as the ratio ρ(300 K)/ρ(40 K) are reported in Table I. Both doped samples show a T_c reduction.

The upper critical field value was determined from the intersection between the tangent to the transition curve through the inflection point and the extrapolated normal-state resistivity. The corresponding temperature in the (T, B) diagram will be henceforth labeled as onset temperature. The irreversibility field was determined from the intersection between the tangent to the transition curve through the inflection point and the baseline $\rho = 0$.

3. Experimental results and discussion

3.1. Upper critical field anisotropy factor

In polycrystalline samples the intrinsic anisotropy of the MgB_2, limiting the sample cross-section active in carrying current, can be considered responsible for the strong decrease of the critical current in magnetic field. MgB_2 polycrystalline samples can be indeed modeled as an ensemble of randomly oriented grains with the same properties and whose upper critical field only depends on the angle θ between the *c* axis of the MgB_2 grain cell and the applied magnetic field direction [5, 38]. The measured upper critical field corresponds to the upper critical field of the grains oriented in such a way that their *c* axis is perpendicular to the applied field direction ($\theta = \pi/2$): these grains first become superconducting upon cooling. By continuing to decrease the temperature in a given external field, also grains with $\theta < \pi/2$ start to become superconducting. Accounting for this phenomenological percolation theory [38] the resistivity drops to zero as soon as a first continuous superconducting current path occurs, i.e. when the fraction of superconducting grains overcomes a critical value labeled as percolation threshold, p_c [43]. The irreversibility field, B_{irr}, can be then identified as B_{c2} (θ_c), i.e. the upper critical field of the grains whose *c* axis forms a θ_c angle with the applied field ($p_c = \cos(\theta_c)$ for randomly oriented grains). Therefore in the framework of the anisotropic Ginzburg-Landau theory [44] B_{irr} can be written as:

$$B_{irr} = B_{c2}(\theta_c) = \frac{B_{c2}(\pi/2)}{\sqrt{\gamma^2 \cos^2(\theta_c) + \sin^2(\theta_c)}} = \frac{B_{c2}(\pi/2)}{\sqrt{(\gamma^2 - 1)\cos^2(\theta_c) + 1}} = \frac{B_{c2}(\pi/2)}{\sqrt{(\gamma^2 - 1)p_c^2 + 1}}$$

where γ is the upper critical field anisotropy factor defined as B_{c2} $(\theta = \pi/2)$ / B_{c2} $(\theta = 0)$ and B_{c2} $(\theta = \pi/2)$ and B_{c2} $(\theta = 0)$ are the upper critical fields of the grains with c axis perpendicular and parallel to the applied field direction, respectively. Thus γ is calculated from the experimental values of B_{c2} and B_{irr} as:

$$\gamma = \frac{1}{p_c}\sqrt{\left(\frac{B_{c2}(T)}{B_{irr}(T)}\right)^2 + p_c^2 - 1} \qquad (3.1)$$

In figure 1 the ratios between the SiC-doped sample and the undoped sample γ values and between the Co-doped sample and the undoped sample γ values are reported as a function of the reduced temperature. For γ evaluation we always assumed p_c = 0.3117, which represents the critical packing factor for a three-dimensional cubic-site system [45, 46]. To take into account that the resistive transition broadening can be due also to other causes such as material inhomogeneities or thermal fluctuations and since the anisotropy contribution disappears in zero applied field (B_{c2} $(\theta = \pi/2)$ = B_{c2} $(\theta = 0)$), we shifted the $B_{irr}(T)$ values introduced in (3.1) of a quantity equal to the transition broadening measured in zero external field (by coarsely assuming that the other contributions to the transition width do not significantly change with magnetic field and temperature).

Both SiC and Co doping-induced defects contribute to reduce γ with respect to the undoped sample in a reduced temperature range corresponding to the absolute temperature range 20-30 K, i.e. in the temperature range more interesting for applications [47].

For the SiC doped sample this anisotropy factor decreasing, joined to the upper critical field shift toward higher temperature (see figure 3) means a clear enlargement of the (B, T) application range. On the contrary for the analyzed Co-dopant percentage the advantage of the anisotropy decrease are partially shadowed by the lowering of the irreversibility and of the upper critical fields (see figure 4).

In agreement with [48] such lowering could be ascribed to local modifications of the condensate due to the presence of magnetic moments.

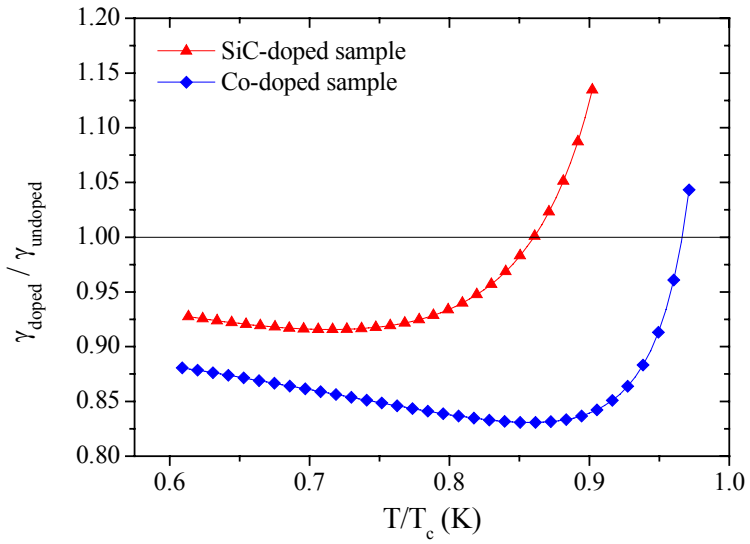

Figure 1. Ratios between the SiC-doped sample and the undoped sample γ values and between the Co-doped sample and the undoped sample γ values.

3.2. Band scattering rates and electronic diffusivities

3.2.1. *SiC doped samples*. Resistivity curves of typical undoped and low-level SiC-doped samples in the range from 25 K up to room temperature and in a magnetic field of 1 Tesla are reported in figures 2(a) and 2(b), respectively.

These curves were obtained by a suitable rescaling of the resistivity measured data in order to take into account the effective grain connectivity. This procedure is based on the hypothesis that fully connected MgB_2 should have a difference in the resistivity values between 300 and 40 K, $\Delta\rho_{sc}$, similar to that of a single crystal [49]. As suggested in [50] we assumed $\Delta\rho_{sc}$ = 8.5 μΩ cm. The resistivity of the connected portions of the samples was then calculated as $\rho_c(T) = \rho(T)\cdot\Delta\rho_{sc}/\Delta\rho$, where $\rho(T)$ is the experimental resistivity curve and the scaling factor $\Delta\rho_{sc}/\Delta\rho$ represents the active fractional area. We found $\Delta\rho_{sc}/\Delta\rho$ = 0.24 and 0.20 for the undoped and SiC-doped sample, respectively.

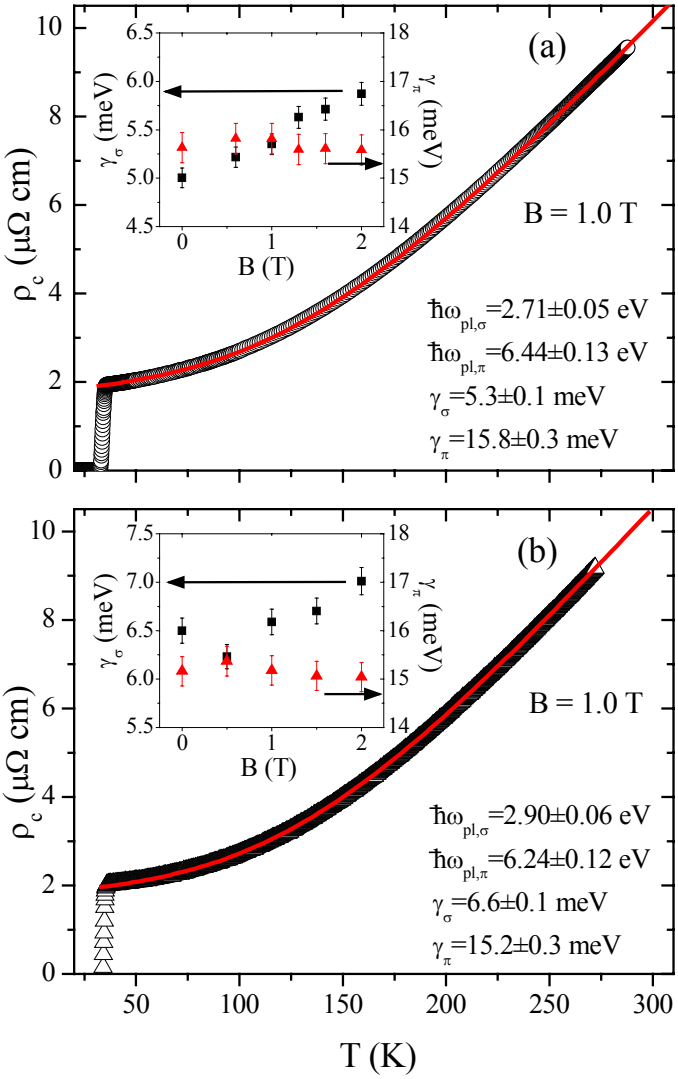

Figure 2. Main frames: temperature dependent rescaled resistivity curves evaluated for undoped (a) and SiC doped (b) samples in an applied magnetic fields B = 1 T (symbols: rescaled experimental data, full lines: fit with (A.1) - see Appendix A). Insets: magnetic field dependence of the σ and π band impurity scattering rates of undoped (a) and SiC doped (b) samples.

In order to evaluate the band scattering rates the ρ_c vs. T curves were fitted in the framework of the two-band model proposed by Mazin *et al.* [29] where we introduced transport spectral functions suitably calculated from the standard Eliashberg functions. More details are reported in Appendix A. Data were fitted by (A.1) where the plasma energies in σ and π bands, $\hbar\omega_{pl,\sigma}$, $\hbar\omega_{pl,\pi}$, as well as the band impurity scattering rates, γ_σ and γ_π were considered free fitting parameters. The fitting curves reproduce the experimental data measured both in zero and in applied magnetic field with great accuracy (figure 2). As expected in samples where no preferential orientation is present, for both the investigated samples the plasma energy values are in good agreement with the average over the three crystallographic directions of the values calculated by Brinkman *et al.* [51], $\hbar\omega_{pl,\sigma} = 3.40$ eV and $\hbar\omega_{pl,\pi} = 6.28$ eV. The plasma energy parameters were kept equal for the zero-field and in-field resistivity analysis.

As expected [56] for both the samples we found $\gamma_\sigma < \gamma_\pi$. Taking into account that in both the samples the critical temperature is close to the theoretical one, we can deduce that the interband scattering rate is very small and γ_σ and γ_π indicate the σ and π intraband scattering rates, respectively.

SiC-doping induces an increase of γ_σ values, whereas no appreciable change was detected in γ_π (figure 2, insets). This indicates that SiC doping-induced defects mainly affect the σ channel, lowering its contribute to the conductivity. It can be ascribed to the fact that C enters the MgB_2 cells on B places, i.e. on planes where σ band is localized. Taking into account the more anisotropic behaviour of the σ band with respect to the π band, this result fittingly explains the decrease of the upper critical field anisotropy factor discussed in section 3.2.1.

This enhancement of the σ intraband scattering is also consistent with the results of investigations on C-doped MgB_2 single crystals [25, 52].

The lower contribution of the σ band to the conductivity is also confirmed by the analysis of the upper critical field within the model suggested by Gurevich [34] where the impurity scattering is accounted for by the electronic diffusivity tensors D_σ and D_π (see Appendix B for details).

Therefore B_{c2} (T) curves were fitted by the formula (B.1). Since the critical temperatures of both

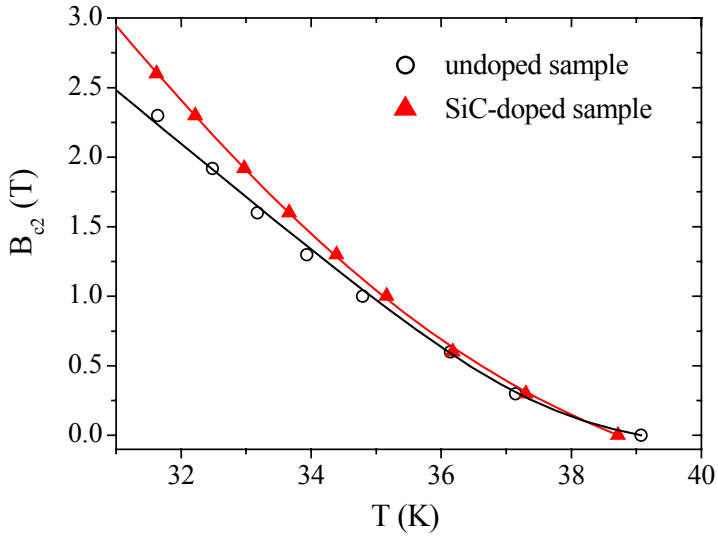

Figure 3. B_{c2} vs. T experimental curves for undoped and SiC-doped bulk samples (symbols). The solid lines are the best fit to the experimental data by (B.1) (see appendix B). Fit parameter values are the following: undoped sample $D_\sigma = (2.56 \pm 0.06)\cdot10^{-4}$ m^2 s^{-1}, $D_\pi = (2.2 \pm 0.6)\cdot10^{-2}$ m^2 s^{-1}; SiC-doped sample $D_\sigma = (2.11 \pm 0.05)\cdot10^{-4}$ m^2 s^{-1}, $D_\pi = (1.9 \pm 0.4)\cdot10^{-2}$ m^2 s^{-1}.

undoped and SiC doped samples are close to the theoretical one, the interband scattering is again assumed negligible. As plotted in figure 3 for both the samples the fitting curves agree very well with the experimental data. We obtained $D_\sigma = (2.56 \pm 0.06)\cdot 10^{-4}$ m^2 s^{-1}, $D_\pi = (2.2 \pm 0.6)\cdot 10^{-2}$ m^2 s^{-1} for the undoped sample and $D_\sigma = (2.11 \pm 0.05)\cdot 10^{-4}$ m^2 s^{-1}, $D_\pi = (1.9 \pm 0.4)\cdot 10^{-2}$ m^2 s^{-1} for the SiC-doped one. This result confirms that SiC doping procedure mainly affect the σ band conduction parameters whereas the difference among the D_π values of the two samples keeps within the experimental errors.

It is worthwhile to note that the decrease of the σ band diffusivity of the SiC-doped sample is (17.6 ± 2.7)% and well agrees, within the experimental errors, with the increase of the σ band scattering rate of (20.9 ± 3.2)% calculated from the normal state resistivity.

3.2.2. Co doped samples – In order to investigate Co-doping influence on band scattering parameters we analyzed the upper critical field dependence on temperature (figure 4) by applying the two-band s-wave Eliashberg equations for $B_{c2}(T)$ [53] where we introduced the terms concerning the band scatting rate from non-magnetic and magnetic impurities as detailed in Appendix C.

By fitting the upper critical field curve of the undoped sample with the equation system (C.1)-(C.2), where the scattering rate parameters due to magnetic impurities are put equal to zero, we obtained the two-band Fermi velocity: $v_{F\sigma} = 3.8\cdot 10^5$ m/s and $v_{F\pi} = 1.8\cdot 10^6$ m/s. Then we reconstruct the upper critical field curve of the Co-doped sample by applying again (C.1) and (C.2) where the above evaluated two-band Fermi velocities as well as the other parameters already used for the undoped sample B_{c2} fit were inserted. Since even very small values of the magnetic impurity scattering rates (i.e. small amount of magnetic disorder) is expected to strongly decrease T_c [54] and the T_c decrease measured in our Co-doped sample is lower than 3 K, we argue that the effective Co amount entered the MgB_2 cells could be much lower than the nominal one. Thus we used in the calculus the same

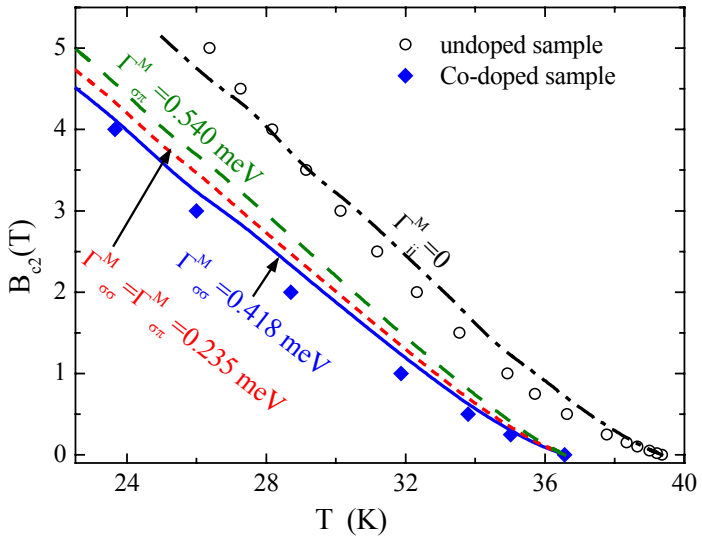

Figure 4. B_{c2} vs. T experimental curves for undoped and Co-doped bulk samples (symbols). The dashed-dotted line is the fit of the experimental data of the undoped sample by the equation system (C.1)-(C.2) (see Appendix C). The other lines are the theoretical curves reconstructed by imposing $\Gamma^M_{\sigma\pi}$ = 0.540 meV, $\Gamma^M_{\sigma\sigma}$= $\Gamma^M_{\pi\pi}$ = 0 (dashed curve), $\Gamma^M_{\sigma\pi}$=$\Gamma^M_{\sigma\sigma}$ = 0.235 meV; $\Gamma^M_{\pi\pi}$ (short-dashed curve) and $\Gamma^M_{\sigma\sigma}$ = 0.418 meV, $\Gamma^M_{\sigma\pi}$= $\Gamma^M_{\pi\pi}$ = 0 (solid curve). The Γ^M_{ij} values used in the calculus were determined imposing the coincidence of the experimental and the theoretical onset temperature at zero-field.

electron-phonon coupling constants and normal densities of states used for the undoped sample.

We hypothesized three different scenarios ascribing the upper critical field lowering 1) to an increase of the only interband magnetic scattering rate ($\Gamma^{\mathrm{M}}_{\sigma\pi} \neq 0$, $\Gamma^{\mathrm{M}}_{\sigma\sigma} = \Gamma^{\mathrm{M}}_{\pi\pi} = 0$), 2) to an equal increase of the interband and of the σ-intraband magnetic scattering rate ($\Gamma^{\mathrm{M}}_{\sigma\pi} = \Gamma^{\mathrm{M}}_{\sigma\sigma}$, $\Gamma^{\mathrm{M}}_{\pi\pi} = 0$), 3) to an increase of the only σ-intraband magnetic scattering rate ($\Gamma^{M}_{\sigma\sigma} \neq 0$, $\Gamma^{\mathrm{M}}_{\sigma\pi} = \Gamma^{\mathrm{M}}_{\pi\pi} = 0$). The corresponding theoretical curves are reported in figure 4 superimposed to the experimental data. The magnetic band scattering values indicated in the figure and used in the calculus were determined imposing the coincidence of the experimental and the theoretical onset temperature at zero field. It is worthwhile to mention that an increase of the π band scattering rate affects very slightly the onset temperature value and therefore cannot be responsible of the B_{c2} curve shift [55].

The assumption that the Co addition increases the σ band scattering rate gives the theoretical curve that better describes the B_{c2} behavior of the doped sample. Therefore we conclude that also magnetic impurities induced by Co-addition mainly affect the σ channel justifying the decrease of the upper critical field anisotropy factor reported in section 3.2.1.

This decrease of the σ band conductivity induced by Co-doping well agree with the outputs obtained from previous studies on disorder induced by Mn magnetic impurity introduction in MgB_2 single crystals [54].

4. Conclusion

A combined electrical transport analysis of superconducting and normal-state properties of MgB_2 polycrystalline samples with two different doping-induced disorder typologies was performed in order to study the doping influence on the magnetic anisotropy of MgB_2 polycrystalline samples and to correlate this influence with the doping-induced changes in band scattering processes. Non magnetic (SiC) and magnetic (Co) dopant effects were investigated.

In both cases nanoparticle addition results in a decrease of the MgB_2 upper critical field anisotropy factor especially in the temperature range 20-30 K more interesting for applications. For SiC-doped samples this result, joined to the upper critical field shift toward higher temperatures, brings to an enlargement of the (B, T) application range whereas in Co doped samples the anisotropy decrease advantage is partially shadowed by the B_{c2} decrease.

According to this scenario the analysis of the normal state resistivity performed on SiC doped samples as well as of the study of the upper critical field dependence on temperature performed on SiC and Co doped samples shows an increases in the σ intraband scattering processes whereas the conductivity of the more isotropic π band remains almost unaffected.

The analysis of the influence of the impurities induced by new doping typologies on intra- and inter-band scattering processes are in progress. Namely correlations between macroscopic dopant-induced effects on electrical transport properties and disorder-induced changes in the band conduction regime are a needed step for the development of doping procedures in polycrystalline samples aimed at more competitive technological applications.

Acknowledgement

This work was supported by MIUR under PRIN project No.2007AW2K4Y.

Appendix A

In the two-band model proposed by Mazin *et al.* [29] the formula for the conductivity can be written as:

$$\frac{1}{\rho_{\mathrm{c}}(T)} = \frac{\varepsilon_0}{\hbar} \sum_{i,j=\sigma,\pi} \frac{\left(\hbar\omega_{\mathrm{pl},i}\right)^2}{\gamma_i + W'_{ij}(T)} \qquad (A.1)$$

where

$$W'_{ij}(T)=(4\pi k_B T)\int_0^{\infty} d\omega \left[\frac{\hbar\omega/2k_B T}{\sinh(\hbar\omega/2k_B T)}\right]^2 \frac{\left[\alpha_{tr}^2(\omega)F'_{tr,ii}(\omega)+\alpha_{tr}^2(\omega)F'_{tr,ij}(\omega)\right]}{\omega}$$

$\gamma_i = \Gamma_{ij} + \Gamma_{ii}$ is the sum of the inter- (Γ_{ij}) and intra- (Γ_{ii}) band impurity scattering rate present in the Eliashberg equations [56], $\hbar\omega_{pl,i}$ is the plasma energy for the i-band and $\alpha_{tr}^2F'_{tr,ij}(\omega)$ are the transport electron-phonon spectral functions tightly connected with the superconducting electron phonon spectral functions [57, 58]. Since transport spectral functions $\alpha_{tr}^2F'_{tr,ij}(\omega)$ have a similar behaviour to that of the standard Eliashberg functions $\alpha^2F_{ij}(\omega)$ except at low frequency where $\alpha_{tr}^2F'_{tr,ij}(\omega)$ behave as ω^4, we defined $\alpha_{tr}^2F'_{tr,ij}(\omega) = b_{ij}\left(c_{ij}\omega^4\,\theta\left(\frac{k_B T_D}{10}-\omega\right)+\alpha^2F_{ij}(\omega)\theta\left(\omega-\frac{k_B T_D}{10}\right)\right)$ where θ is the Heaviside function, T_D is the Debye temperature and b_{ij} are normalizing constants [41]. The constants c_{ij} were determined in such a way to guarantee the continuity of the spectral functions.

Appendix B

In the framework of the model elaborated by Gurevich [34], by assuming the interband scattering negligible, $B_{c2}(T)$ curves were fitted by the formula:

$$a_0[\ln t + U(h)][\ln t + U(\eta h)] + a_2[\ln t + U(\eta h)] + a_1[\ln t + U(h)] = 0 \qquad (B.1)$$

where $t = T/T_c$, $U(x) = \Psi(1/2 + x) - \Psi(x)$, $h = \frac{B_{c2}\hbar\sqrt{D_\sigma(\theta)}}{2\phi_0 k_B T_c t}$, $\eta = \frac{D_\pi(\theta)}{D_\sigma(\theta)}$, $\Psi(x)$ is the logarithmic derivative of the Euler gamma function, ϕ_0 is the magnetic flux quantum, $D_{\sigma,\pi}(\theta)$ are the electronic diffusivities of the σ and π bands, respectively, and θ is the angle between the c-axis of the MgB_2 cell and the applied magnetic field direction. a_0, a_1, a_2 are constants derived from the superconducting coupling constants, λ_{ij}, determined from *ab initio* calculations [57]. Since our samples are polycrystalline the measured B_{c2} values provide the upper critical field of the grains oriented with their *ab* planes along the applied field. This means that $\theta = \pi/2$ and $D_{\sigma,\pi} = \sqrt{D_{\sigma,\pi}^{ab}D_{\sigma,\pi}^{c}}$, where $D_{\sigma,\pi}^{ab}$ and $D_{\sigma,\pi}^{c}$ are the in-plane and out-of-plane diffusivities, respectively.

Appendix C

By following the microscopic model reported in Refs. 31-33 and taking into account the presence of magnetic impurities inside the Co-doped sample the two-band s-wave Eliashberg equations can be written as:

$$\omega_n Z_i(i\omega_n) = \omega_n + \pi T\sum_{m,j}\Lambda_{ij}(i\omega_n - i\omega_m)\,\mathrm{sign}(\omega_m) + \sum_j\left(\Gamma_{ij}^N + \Gamma_{ij}^M\right)\mathrm{sign}(\omega_n) \qquad (C.1)$$

$$Z_i(i\omega_n)\Delta_i(i\omega_n) = \pi T\sum_{m,j}\left[\Lambda_{ij}(i\omega_n - i\omega_m) - \mu_{ij}^*(\omega_c)\right]\theta(|\omega_c| - \omega_m)\,\chi_j(i\omega_m)\,Z_j(i\omega_m)\Delta_j(i\omega_m) + \\ + \sum_j\left(\Gamma_{ij}^N - \Gamma_{ij}^M\right)\chi_j(i\omega_n)\,Z_j(i\omega_n)\Delta_j(i\omega_n) \qquad (C.2)$$

where i and j are the band indices, $\omega_n = \pi T(2n\text{-}1)$ ($n = 0,\pm1, \pm2,\ldots$) the Matsubara frequencies, ω_c a cut-off frequency, Γ_{ij}^N and Γ_{ij}^M the non-magnetic and the magnetic impurity scattering rates,

respectively, $\mu^*_{ij}(\omega_c)$ the Coulomb pseudopotential [32], θ the Heaviside function, and $\Delta_j(\mathrm{i}\omega_n)$ and $Z_j(\mathrm{i}\omega_n)$ the superconductive gap and the renormalization function of the *j* band, respectively. Finally $\Lambda_{ij}(\mathrm{i}\omega_n - \mathrm{i}\omega_m) = \int_0^\infty d\omega\, \alpha^2_{ij}F(\omega) \Big/ \left[(\omega_n - \omega_m)^2 + \omega^2\right]$ - where $\alpha^2_{ij}F(\omega)$ are the standard Eliashberg functions [57] – and $\chi_j(\mathrm{i}\omega_m) = \left(2/\sqrt{\beta_j}\right) \int_0^\infty \mathrm{d}q \exp\left(-q^2\right) \tan^{-1}\left\{ q\sqrt{\beta_j} \Big/ \left[\left|\omega_m Z_j(\mathrm{i}\omega_m)\right| + \mathrm{i}\mu_B B_{c2}\, \mathrm{sign}(\omega_m)\right]\right\}$ - where $\beta_j = \pi B_{c2}\, v^2_{Fj} / (2\phi_0)$, v_{Fj} is the Fermi velocity of the *j* band, μ_B the Bohr magneton and ϕ_0 the flux quantum.

References

[1] Liu A Y, Mazin I I and Kortus J 2001 *Phys. Rev. Lett.* **87** 087005
[2] Vinod K, Varghese N and Syamaprasad U 2007 *Supercond. Sci. Technol.* **20** R31-45
[3] Xi X X 2008 *Rep. Prog. Phys.* **71** 116501
[4] Ghigo G, Botta D, Chiodoni A, Gozzelino L, Gerbaldo R, Laviano F, Mezzetti E, Monticone E and Portesi C 2005 *Phys. Rev.* B **71** 214522
[5] Eisterer M 2007 *Supercond. Sci. Technol.* **20** R47-73
[6] Wilke R H T, Bud'ko S L, Canfield P C, Finnemore D K, Suplinskas R J and Hannahs S T 2004 *Phys. Rev. Lett.* **92** 217003
[7] Kovàč P, Hušek I, Skàkalova V, Meyer J, Dobročka E, Hirscher M and Roth S 2007 *Supercond. Sci. Technol.* **20** 105-11
[8] Ma Y, Zhang X, Nishijima G, Watanabe K, Awaji S and Bai X 2006 *Appl. Phys. Lett.* **88** 072502
Zhang X, Wang D, Gao Z, Wang L, Ma Y, Qi Z and Watanabe K, 2008 *Supercond. Sci. Technol.* **21** 075008
[9] Serrano G, Serquis A, Dou S X, Soltanian S, Civale L, Maiorov B, Holesinger T G, Balakirev F and Jaime M 2008 *J. Appl. Phys.* **103** 023907
[10] Yan S C, Yan G, Zhou L, Jia Y, Wen H H and Lu Y F 2007 *Supercond. Sci. Technol.* **20** 377-80
[11] Braccini V, Gurevich A, Giencke J E, Jewell M C, Eom C B, Larbalestier D C, Pogrebnyakov A, Cui Y, Liu B T, Hu Y F, Redwing J M, Li Qi, Xi X X, Singh R K, Gandikota R, Kim J, Wilkens B, Newman N, Rowell J, Moeckly B, Ferrando V, Tarantini C, Marrè D, Putti M, Ferdeghini C, Vaglio R and Haanappel E 2005 *Phys. Rev.* B **71** 012504
[12] Kim J H, Zhou S, Hossain M S A, Pan A V and Dou S X 2006 *Appl. Phys. Lett.* **89** 122510
[13] Gao Z, Ma Y, Zhang X, Wang D, Yu Z, Yang H, Wen H and E. Mossang 2007 *J Appl. Phys.* **102** 013914
[14] Hossain M S A, Kim J H, Wang X L, Xu X, Peleckis G and Dou S X 2007 *Supercond. Sci. Technol.* **20** 112-6
Hossain M S A, Senatore C, Flükiger R, Rindfleisch M A, Tomsic M J, Kim J H and Dou S X 2009 *Supercond. Sci. Technol.* **22** 095004
[15] Dou S X, Shcherbakova O, Yeoh W K, Kim J H, Soltanian S, Wang X L, Senatore C, Flukiger R, Dhalle M, Husnjak O and Babic E 2007 *Phys. Rev. Lett.* **98** 097002
Wang J L, Zeng R, Kim J H, Lu L and Dou S X 2008 *Phys. Rev. B* **77** 174501
[16] Vajpayee A, Awana V P S, Bhalla G L and Kishan H 2008 *Nanotechnology* **19** 125708
[17] Yamamoto A, Shimoyama J, Ueda S, Iwayama I, Horii S and Kishio K 2005 *Supercond. Sci. Technol.* **18** 1323-28
[18] Lezza P, Senatore C and Flükiger R 2006 *Supercond. Sci. Technol.* **19** 1030-33
[19] Shen T M, Li G, Cheng C H and Zhao Y 2006 *Supercond. Sci. Technol.* **19** 1219-24
[20] Shekhar C, Giri R, Tiwari R S, Srivastava O N and Malik S K 2007 *J Appl. Phys.* **101** 043906
[21] Kimishima Y, Sugiyama Y, Numa S, Uehara M and Kuramoto T 2008 *Physica* C **468** 1185-7
[22] Prikhna T A, Gawalek W, Savchuk Ya M, Moshchil V E, Sergienko N V, Surzhenko A B,

Wendt M, Dub S N, Melnikov V S, Schmidt Ch, Nagorny P A 2003 *Physica* C **386** 565
[23] Gozzelino L, Gerbaldo R, Ghigo G, Laviano F, Lopardo G, Ummarino G A, Giunchi G, Perini E, Bassani E, Agostino A and Minetti B 2009 *IEEE Trans. Appl. Supercond.* **19** 3524-7
[24] Giunchi G, Perini E, Orecchia C, Ripamonti G, Bassani E, Carcano G, DeMarzi G, Viola R, Turtù S 2009 *IEEE Trans. Appl. Supercond.* **19** 2802-6
[25] Sologubenko A V, Zhigadlo N D, Kazakov S M, Karpinski J and Ott H R 2005 *Phys. Rev.* B **71** 020501
[26] Drozd V A, Gabovich A M, Gierłowski P, Pękała M and Szymczak H 2004 *Physica* C **402** 325-34
[27] Kim K H, Choi J- H, Jung C U, Chowdhury P, Lee H- S, Park M- S, Kim H- J, Kim J Y, Du Z, Choi E- M, Kim M- S, Kang W N, Lee S- I, Sung G Y and Lee J Y 2002 *Phys. Rev.* B **65** 100510
[28] Putti M, Braccini V, Galleani E, Napoli F, Pallecchi I, Siri A S, Manfrinetti P and Palenzona A 2003 *Supercond. Sci. Technol.* **16** 188-62
[29] Mazin I I, Andersen O K, Jepsen O, Dolgov O V, Kortus J, Golubov A A, Kuz'menko A B and van der Marel D 2002 *Phys. Rev. Lett.* **89** 107002
[30] Bugoslavsky Y, Miyoshi Y, Perkins G K, Caplin A D, Cohen L F, Zhai H Y, Christen H M, Pogrebnyakov A V, Xi X X and Dolgov O V 2004 *Supercond. Sci. Technol.* **17** S350-4
[31] Shulga S V, Drechsler S- L, Fuchs G, Müller K- H, Winzer K, Heineke M and Krug K 1998 *Phys. Rev. Lett.* **80** 1730-3
[32] Ummarino G A 2005 *Physica* C **423** 96-102
[33] Suderow H, Tissen V G, Bristol J P, Martínez J L, Vieira S, Lejay P, Lee S and Tajima S 2004 *Phys. Rev.* B **70** 134518
[34] Gurevich A 2003 *Phys. Rev.* B **67** 184515
[35] Gobulov A A and Koshelev A E 2003 *Phys. Rev.* B **68** 104503
[36] Giunchi G 2003 *Intern. J. Mod. Phys.* B **17** 453-60
[37] Giunchi G, Ripamonti G, Cavallin T and Bassani E 2006 *Cryogenics* **46** 237-42
[38] Eisterer M, Zehetmayer M, Weber H W 2003 *Phys. Rev. Lett.* 90 247002
Eisterer M, Krutzler C, Weber H W 2005 *J. Appl. Phys.* **98** 033906
[39] Giunchi G, Ceresara S, Ripamonti G, Chiarelli S and Spadoni M 2003 *IEEE Trans. Appl. Supercond.* **13** 3060-3
[40] Dou S X, Pan A V, Zhou S, Ionescu M, Wang X L, Horvat J, Liu H K and Munroe P R 2003 *J. Appl. Phys.* **94** 1850-6
[41] Gozzelino L, Minetti B, Ummarino G A, Gerbaldo G, Ghigo G, Laviano F, Lopardo G, Giunchi G, Perini E, Mezzetti E 2009 *Supercond. Sci. Technol.* **22** 065007
[42] Shi L, Zhanga S and Zhang H 2008 *Solid St. Comm.* **147** 27-30
[43] Zeimetz B B, Glowacki B A and Evetts J E 2002 *Eur. Phys. J.* B **29** 359
[44] Tilley D R 1965 *The Ginzburg-Landau equations for anisotropic alloys*: *Proc. Phys. Soc.* vol 86 pp. 678-9
[45] Yamamoto A, Shimoyama J, Kishio K, Matsushita T 2007 *Supercond. Sci. Technol.* **20** 658-66
[46] Heermann D W, Stauffer D 1980 *Z. Phys. B* **40** 39-44
[47] Vinod K, Abhilash Kumar R G and Syamaprasad U 2007 *Supercond. Sci. Technol.* **20** R1-13
[48] Lange M, Van Bael M J and Moshchalkov V V 2003 *Phys. Rev.* B **68** 174522
[49] Rowell J M 2003 *Supercond. Sci. Technol.* **16** R17-27
[50] Tarantini C, Aebersold H U, Braccini V, Celentano G, Ferdeghini C, Ferrando V, Gambardella U, Gatti F, Lehmann E, Manfrinetti P, Marrè D, Palenzona A, Pallecchi I, Sheikin I, Siri A S and Putti M 2006 *Phys. Rev.* B **73** 134518
[51] Brinkman A, Golubov A A, Rogalla H, Dolgov O V, Kortus J, Kong Y, Jepsen O and Andersen O K 2002 *Phys. Rev.* B **65** 180517
[52] Masui T, Lee S and Tajima S 2004 *Phys. Rev.* B **70** 024504
[53] Prohammer M and Schachinger E 1987 *Phys. Rev.* B **36** 8353

[54] Gonnelli R S, Daghero D, Ummarino G A, Calzolari A, Tortello M, Stepanov V A, Zhigadlo N D, Rogacki K, Karpinski J, Bernardini F, Massidda S 2006 *Phys. Rev. Lett.* **97** 037001
[55] Ummarino G A 2007 *J. Supercond.* **20** 639-42
[56] Dolgov O V, Kremer R K, Kortus J, Golubov A A and Shulga S V 2005 *Phys. Rev.* B **72** 024504
[57] Golubov A A, Kortus J, Dolgov O V, Jepsen O, Kong Y, Andersen O K, Gibson B J, Ahn K and Kremer R K 2002 *J. Phys.: Condens. Matter* **14** 1353-60
[58] Allen P B 1978 *Phys. Rev.* B **17** 3725-34